CHEMISTRY OF MATERIALS

ARTICLE

pubs.acs.org/cm

Role of Lattice Distortions in the Oxygen Storage Capacity of Divalently Doped CeO_2

Aoife B. Kehoe, David O. Scanlon,* and Graeme W. Watson*

School of Chemistry and CRANN, Trinity College Dublin, Dublin 2, Ireland

ABSTRACT: The doping of ceria (CeO_2) with divalent noble metal ions has been shown to improve the reducibility and enhance the oxygen storage capacity (OSC), although the reasons for this are not well understood. We have examined the interaction of a range of divalent dopants with CeO_2 using density functional theory, and found that the dopant preferentially adopts the coordination of its own oxide, instead of the cubic coordination of Ce(IV) in ceria. Depending on the electronic structure of the dopants, the different coordinations can create weakly- or under-coordinated oxygen ions that are more easily removed than in pure CeO_2. We have used these insights to identify dopants which will increase the reducability of CeO_2, while being economically more viable than the presently used noble metals, and we outline guidelines for the design of improved oxide catalysts.

KEYWORDS: CeO_2, doping, vacancy, ceria, catalysis, defects

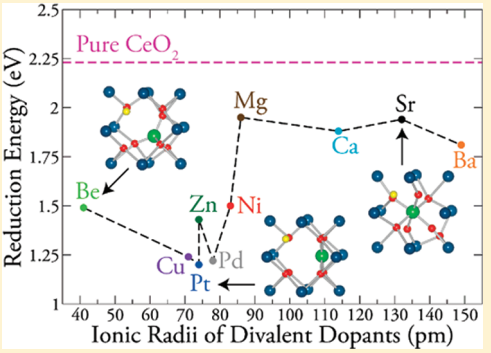

INTRODUCTION

Ceria has long been regarded as one of the key materials in modern catalysis, and has been highly effective in the catalysis of automotive emissions, both as a support and as a catalyst itself.[1−3] The importance of ceria as a catalyst and as a support stems from its oxygen storage capacity (OSC), which allows it to release oxygen under reducing conditions and to store oxygen by filling oxygen vacancies under oxidizing conditions.[4,5] The high OSC of ceria is facilitated by the ease with which Ce ions can be reduced upon oxygen vacancy formation. The Ce ions undergo a relatively facile reduction from Ce^{IV} to Ce^{III}, a process which occurs via the removal of an oxygen atom, with the localization of the two remaining electrons into the 4f states of two adjacent Ce ions.[3] In Kröger-Vink notation, the process is written as

$$O_O^x + 2Ce_{Ce}^x \rightarrow V_O^{\bullet\bullet} + 2Ce'_{Ce} + \frac{1}{2}O_2(g) \qquad (1)$$

where O_O^x and Ce_{Ce}^x are neutral O and Ce on their respective lattice sites, $V_O^{\bullet\bullet}$ is vacancy on an oxygen site with an effective charge of +2, and Ce'_{Ce} denotes a Ce on a Ce site with an effective charge of −1, i.e., formally a Ce^{III} ion.

The stringent environmental regulations being imposed around the world have fueled the need for more efficient catalysts, and to this end the doping of ceria has gained much interest. Recently doping of ceria with noble metals (Pd, Pt etc.), that normally sit atop CeO_2 supports in three-way catalysts (TWCs), has emerged as a promising route to improved catalysts, and has been termed "noble metal ionic catalysis".[6] It is widely acknowledged that these noble metals (Cu, Pd, Pt) enter the CeO_2 lattice in their 2+ oxidation states and cause the spontaneous formation of a charge compensating oxygen vacancy (CCV), which has been evidenced in Extended X-ray absorption fine structure (EXAFS) and X-ray photoelectron spectroscopy (XPS) studies.[7−9] The description of the substitution of the divalent dopant M into the lattice and the formation of the CCV is given (in Kröger-Vink notation) by

$$MO + O_O^x + Ce_{Ce}^x \rightarrow V_O^{\bullet\bullet} + M''_{Ce} + CeO_2 \qquad (2)$$

It should be noted that CCV formation is not a reduction that contributes to the OSC, but is a consequence of the system maintaining charge neutrality as part of the doping process.

Experimentally, $Ce_{1-x}Pd_xO_{2-\delta}$ and $Ce_{1-x}Pt_xO_{2-\delta}$ have been reported to catalyze CO oxidation, hydrocarbon oxidation, and NO_x reduction.[6] $Ce_{1-x}Cu_xO_{2-\delta}$ has found catalytic applications in processes such as NO reduction[10] and CO oxidation,[11] and $Ce_{1-x}Ni_xO_{2-\delta}$ has been shown to catalyze methane oxidation[12] and the water−gas shift (WGS) reaction.[13] Ni, Pd, Pt, and Cu have been previously examined computationally as ceria dopants with a view to understanding the increased catalytic activity,[14−18] but many of these studies failed to account for the CCV, whereas some reported the formation energy of the CCV to be the reduction energy[16,17] as opposed to an intrinsic component of the doping process.

One of the key concepts when doping CeO_2 or any other oxide to increase the reducibility, is the size of the dopant. Doping with a cation that is smaller than the host cation can create both short and long metal−oxygen bonds, with the oxygen atoms bonded by long bonds to the metal being weaker, and therefore easier to remove. This has been demonstrated previously for Ti and Zr-doped CeO_2,[19,20] and in a previous study of Pd- and Pt-doped CeO_2.[21]

Recently, we have shown using density functional theory (DFT) that the origin of the enhanced reducibility of Pd/Pt

Received: June 8, 2011
Revised: September 8, 2011
Published: September 20, 2011

ACS Publications © 2011 American Chemical Society

doped CeO_2 is mediated by large lattice distortions that the dopants undergo within the CeO_2 lattice.[22] Pd and Pt distort by ~1.2 Å from the perfect Ce lattice position to assume a square planar coordination with four of the neighboring oxygen ions.[22] Interestingly square planar coordination is the coordination adopted by Pt and Pt in their respective binary oxides, PdO and PtO. These distortions leave three under-coordinated oxygen atoms, which are more facile to remove than O in pure CeO_2. Square planar coordination of Pd on the low index surfaces of CeO_2 has also recently been reported.[23] These findings beg the question: can the coordination of the binary dopants in their native oxides determine the extent of distortion and therefore the reducibility of divalently doped CeO_2?

In this study, we use DFT to investigate the effect of a range of divalent dopants (Be, Mg, Ca, Sr, Ba, Ni, Cu, Zn, Pd and Pt) on the formation of oxygen vacancies of CeO_2. We show (i) that in all cases, the dopant ions distort to adopt the coordination of their own binary oxide, and not that of cubically coordinated Ce in CeO_2 and (ii) the magnitude of the distortion correlates with the increased reducibility of the divalently doped CeO_2. Our results highlight the need to check alternative positions (or broken symmetry starting structures) for dopants in CeO_2 to find the correct ground state, and we propose guidelines for choosing dopants to improve the reducibility of materials.

THEORETICAL SECTION

All our DFT calculations were performed with the Vienna ab initio simulation package (VASP),[24] within which projector augmented wave (PAW) pseudopotentials and a plane wave cutoff of 400 eV were used. Calculations were carried out using the generalized gradient approximation exchange-correlation functional of Perdew, Burke and Ernzerhof[25] with the $+U$ correction of Dudarev[26] to account for on-site Coulombic interactions. Standard density functional calculations are unable to correctly describe the electronic structure of reduced CeO_2,[27,28] due to the self-interaction error inherent to such functionals, which is acute for strongly localized orbitals such as transition metal d or rare earth f states.[29−31] For Ce f states we employ a U value of 5 eV, which has been widely used,[28,32−34] and for the O p states, we employ a U value of 5.5 eV, which was derived using a Koopmans-like approach.[35] This U value for the O 2p states allows for the correct description of localized oxygen holes in CeO_2.[35] Ni(II), Pd(II), Pt(II), and Cu(II) all have partially occupied d shells, so it is necessary to include U parameters for these states to accurately model their behavior. A U value of 5.2 eV was used for the copper ions,[36−38] and a U of 5.3 eV was employed for the Ni(II),[39] as these have been shown to reproduce the valence band features of their native oxides. For palladium and platinum, appropriate U values for the d states were selected by comparison to the d peak in photoemission (XPS) data,[40] with the U parameter used for nickel (U = 5.3 eV) found to be reasonable for these other d^8 ions. A k-point mesh of 2 × 2 × 2 was used for the 96 atom 2 × 2 × 2 supercell. All calculations were spin polarized and were optimized until the residual forces on each ion were less than 0.01 eVÅ^{-1}. In each case, one dopant ion was was placed in a 96 atoms cell, corresponding to a 3.12% doping concentration. The concentrations of oxygen vacancies were 1.56% for a system with a CCV, and 3.12% for a system with a CCV and an active oxygen vacancy.

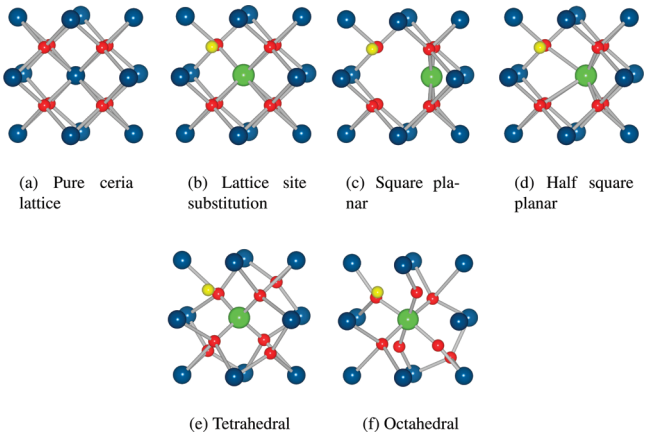

Figure 1. Tested structural configurations of a divalent dopant into ceria. Cerium ions are shown in blue, oxygens in red, the CCV in yellow, and the dopant in green.

Table 1. Energies of various Lattice Distortions Relative to That of the Lowest Energy Configuration for Each Dopant[a]

	lattice site	square planar	half square planar	tetrahedral	octahedral
Be(II)	+2.24	+0.21		0.00	+2.12
Mg(II)	0.00				
Ca(II)	0.00				
Sr(II)	0.00				
Ba(II)	0.00				
Ni(II)		+0.13			0.00
Pd(II)	+0.27	0.00			
Pt(II)	+1.01	0.00			
Cu(II)	+0.74	0.00			
Zn(II)	+0.15		0.08	0.00	+0.13

[a] All systems include a CCV. A dash denotes configurations that relaxed to an alternative arrangement. All values are in eV.

RESULTS

Ceria adopts the fluorite structure, with the Ce ions in cubic coordination and the O ions tetrahedrally coordinated (Figure 1a). The dopant configurations explored were the direct substitution onto a cerium lattice site with cubic coordination (Figure 1b), the dopant in a square planar site (Figure 1c), the dopant in a position halfway between the cubic and square planar sites (Figure 1d), the dopant on the lattice site with tetrahedral coordination (Figure 1e), and the dopant on the lattice site with octahedral coordination (Figure 1f). All of the distortions included a neighboring CCV, consistent with EXAFS.[7−9]

For the group 2 ions, substitution of a Ce(IV) by a M(II) ions results in the formation of two holes in the system. As the valence band maximum of CeO_2 is dominated by O 2p states, these holes localize on oxygen atoms neighboring the dopants, forming small polarons (often called oxygen holes[41,42]). Our Koopman's derived U value[35] for the O 2p states allows us to correctly model these localized states. The formation of a CCV quenches these hole states, making the defects electronically inactive. In all cases, the energy to form a CCV was found to be negative, indicating that a CCV spontaneously forms.

For the group 2 dopants with CCVs, excluding Be(II), it was observed that all of the various distortions relax to the original

dx.doi.org/10.1021/cm201617d |Chem. Mater. 2011, 23, 4464–4468

lattice site configuration (Figure 1b) with some distortions of the M−O bond lengths, making it the only energetically stable configuration for these dopants (also summarized in Table 1). The oxygen ions are arranged around the dopant on the lattice site in a cubic fashion, as they are around the cerium ions, although with one oxygen site vacant (the CCV). For Sr(II) and Ba(II), which are bigger than Ce(IV), the oxygen ions move away from the dopant, increasing the average M−O bond length from 2.37 Å in pure ceria to 2.48 and 2.58 Å, respectively. Ca(II), which is of a similar ionic radius to Ce(IV), only distorts the bond lengths to 2.41 Å, while the smaller Mg(II) dopant pulls the surrounding oxygen ions closer to a distance of 2.32 Å.

In contrast to the rest of the ions in the same group, Be(II) adopts a number of stable configurations, of which the most favorable is tetrahedral coordination. From the initial tetrahedral distortion, the beryllium ion moves 1.04 Å off the lattice site into a distorted tetrahedral (Figure 2). Due to the small ionic radius of Be(II), local minima are found for other distortions involving the displacement of the dopant. The square planar arrangement is 0.21 eV less stable than the distorted tetrahedral, and the Be(II) ion relaxes to the square planar site from the half square planar configuration. Be(II) in an octahedral starting point also relaxed to a square planar arrangement on the lattice site by moving two of the six oxygen away from the dopant, leaving the other four coordinated to the dopant in square planar configuration. However, this configuration is 1.91 eV less stable than placing the dopant on the square planar site. The many local minima found in this case highlights the need for care when attempting to find the lowest energy configuration of dopants in CeO_2.

For the transition metal doped supercells, the formation of a CCV beside the dopant was again found to be spontaneous in each case, consistent with previous experimental findings.[7−9]

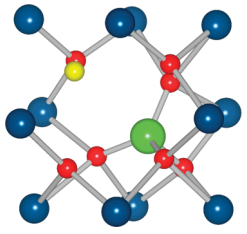

Figure 2. Distorted tetrahedral structure preferentially adopted by Be(II) in ceria.

When doping with transition metals, crystal field splitting effects become important. A transition metal placed on the cubic Ce lattice site will experience a cubic crystal field splitting, Figure 3 a. However, when doped with Pd(II) and Pt(II), the dopants

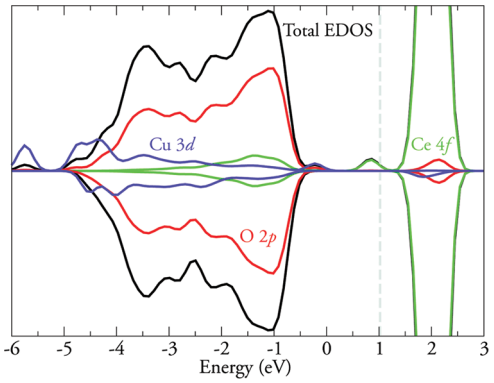

Figure 4. Atom projected electronic densities of states for Cu doped CeO_2 with a charge compensating vacancy and an "active" vacancy. O 2p states are red, Ce 4 f states are green, and Cu 3d states are violet. The top of the valence band is aligned to 0 eV with the vertical dashed line showing the position of the highest occupied state The Cu 3d states have been magnified by a factor of 4 for clarity.

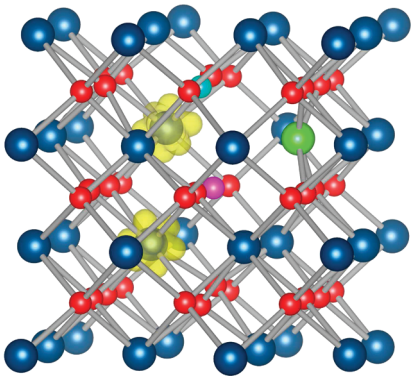

Figure 5. Charge density isosurface of the occupied Ce f defect peak in the band gap of reduced Cu-doped ceria, Figure 4. Ce ions, O ions, the Cu dopant, the CCV, and the reduction vacancy are shown as blue, red, green, turquoise, and magenta, respectively. The isosurface is at 0.05 eV $Å^{-3}$.

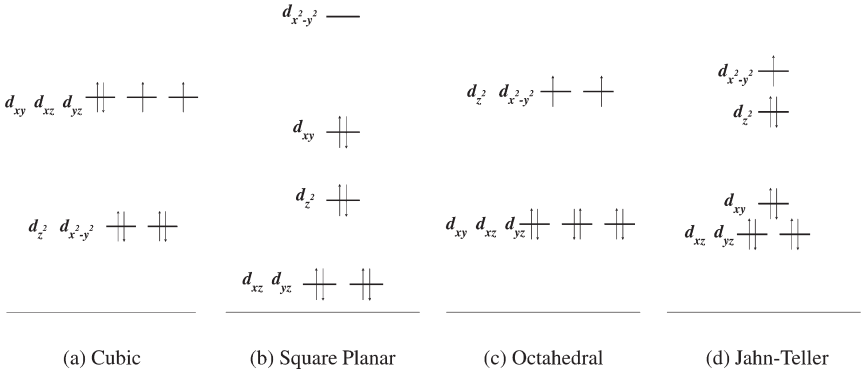

Figure 3. Cubic, square planar, and octahedral crystal field splitting diagram for a d^8 ion, and Jahn−Teller distorted octahedral splitting diagram for a d^9 ion. For Pd(II) and Pt(II), breaking the degeneracy of the high energy t_2 set in the cubic splitting field results in increased stabilization of the system, whereas for Cu(II), a Jahn−Teller like distortion breaks the symmetry without raising the energy of the $d_{x^2-y^2}$ orbital as high as in square planar splitting.

dx.doi.org/10.1021/cm201617d |*Chem. Mater.* 2011, 23, 4464–4468

Table 2. Formation Energy (E_{red}) for an Oxygen Vacancy in Doped CeO_2[a]

	Be(II)	Mg(II)	Ca(II)	Sr(II)	Ba(II)	Ni(II)	Pd(II)	Pt(II)	Cu(II)	Zn(II)
E_{red}	1.49	1.95	1.88	1.94	1.81	1.50	1.22	1.20	1.24	1.43
ΔE_{red}	−0.74	−0.29	−0.35	−0.29	−0.42	−0.73	−1.01	−1.03	−0.99	−0.80

[a] ΔE_{red} denotes the difference in reduction energies between undoped and doped ceria. (Note that E_{red} for pure CeO_2 is 2.23 eV). All values given in eV.

preferentially adopt the square planar configuration as indicated in Figure 1 (b), as is observed in PdO and PtO. The driving force for this is clear from the crystal field splitting shown in Figure 3. Distortion of these d^8 ions from octahedral (Figure 3c) to the square planar arrangement alleviates the degeneracy of the *e* set and results in the pairing of all d electrons so that the highest energy orbital ($d_{x^2-y^2}$) is unoccupied. In its most stable configuration, the Ni(II) system relaxes to a distorted octahedral configuration, remaining on the lattice site but distorting the surrounding oxygen, which is consistent with the coordination of Ni(II) in NiO. The differences in the preferred coordinations of Pd(II)/Pt(II) and Ni(II) can be explained by considering how much more diffuse the 4d and 5d orbitals are than the 3d, meaning that as you move down the group the crystal field splitting increases accordingly. The magnitude of the d−d splitting in Ni(II) is therefore less than for Pd(II) or Pt(II), and it does not achieve the same stabilization by adopting a square planar structure.

Cu(II) undergoes a Jahn−Teller like distortion three-quarters of the way from the perfect lattice site to the square planar site, breaking the degeneracy. However, because it is a d^9 ion, full square planar coordination would be energetically unfavorable as it would require the occupation of the high energy $d_{x^2-y^2}$ orbital, Figure 3d. A similar result has recently been reported by Hermansson and co-workers, although the driving force for the distorted ground state adopted by the Cu ion was not rationalized.[43] Zn(II) is d^{10}, so ligand splitting effects are not relevant, and it stabilizes in the same distorted tetrahedral configuration adopted by Be(II). It is important to note that Be(II), Pd(II), Pt(II), Ni(II), Cu(II), and Zn(II) all adopt the same coordination as in their respective binary oxides when doped in CeO_2.

For all dopants, the subsequent removal of an "active" oxygen vacancy from the doped cells with CCVs (i.e., reduced doped CeO_2) results in the appearance of a defect peak in the band gap in the density of states. In Figure 4 we show the partial ion and orbital decomposed electronic density of states of reduced Cu-doped CeO_2. A distinct occupied Ce f dominated defect state is located ∼0.9 eV below the conduction band. A charge density plot of this defect peak for reduced Cu-doped ceria (Figure 5), shows that the localized electrons surrounds two cerium ions adjacent to the oxygen vacancy, indicating that the two electrons left behind by the removal of an oxygen have localized on two neighboring Ce ions, reducing them from Ce(IV) to Ce(III). This is at variance with previous studies of transition metal doped CeO_2 which have claimed that the reduction process involves the formation of metal induced gap states (MIGS) on doping, which are then quenched with the creation of an oxygen vacancy.[16,17]

The reduction energies for each of the doped systems and their improvement over pure ceria is shown in Table 2. The reduction energy is lower in the presence of all the dopants, when compared to pure CeO_2. It is clear that the magnitude of the decrease in the reduction energy of the doped supercells over that of pure ceria is proportional to the degree of relaxation that the dopant experiences. The improvement is most significant

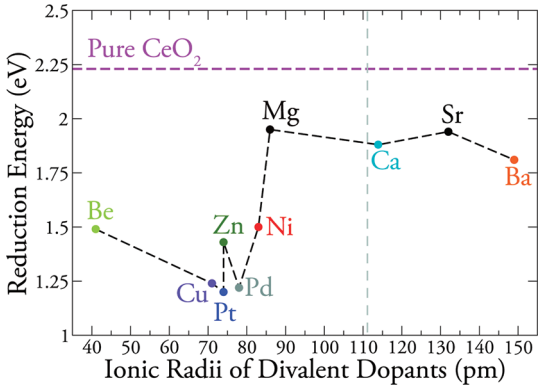

Figure 6. Plot showing the reduction energy for divalently doped CeO_2 against the ionic radii of the divalent dopant. The energy required to reduce pure CeO_2 is indicated by the pink horizontal dashed line. The ionic radii of Ce(IV) is indicated by the vertical gray dashed line.

in the systems in which the dopant undergoes a large lattice distortion and a change in coordination, whereas those in which the dopant remains on the lattice site configuration show the least enhancement. Although the Pd(II) and Pt(II) doped systems show the greatest improvements with reduction energies less than pure ceria by 1.01 eV and 1.03 eV respectively, Be(II), Ni(II), Cu(II) and Zn(II) also show a significant decrease in the reduction energy, improving on that of pure ceria by 0.74, 0.73, 0.99, and 0.80 eV, respectively. It must be noted that in the case of all the dopants considered, it is the Ce(IV) to Ce(III) reduction that occurs, and that the reduction of the oxygen vacancy formation energy is not linked to any MIGS. The role of the dopant is purely to distort the lattice enough to break M−O bonds and create undercoordinated oxygen atoms that can be easily removed.

■ DISCUSSION AND CONCLUSION

At this point it is instructive to rationalize the effect of the driving force of the electronic structure of the dopant, and the effect of the size of the dopant ion. In Figure 6, we have plotted the formation energy of an oxygen vacancy in reduced doped CeO_2 against the ionic radii of the dopants. It is clear that the size of the dopant is a factor, but is not the main factor in lowering the reduction energy. The larger dopants such as Mg, Ca, Sr, and Ba do distort the lattice slightly, but not enough for a significant lowering of the reduction energy. Be, which is the smallest dopant considered, causes a reduction energy that is ∼0.3 eV higher in energy than that of Pt. Zn and Pt have very similar ionic radii, but Pt lowers the reduction energy by ∼0.25 eV relative to Zn. This can be explained by examining the magnitude of the distortion caused by the dopants. Pd and Pt distort by ∼1.2 Å from the perfect lattice site, whereas Zn and Be only distort by ∼1.05 Å, indicating that the magnitude of the distortions is driven by the electronic structure requirements (crystal field effects) of the dopants. Therefore, although size of the dopant

dx.doi.org/10.1021/cm201617d |*Chem. Mater.* 2011, 23, 4464–4468

ion is a factor, the dominant factor is the distortion caused by the electronic structure requirements of the dopants.

Taking into account the improvement in reducibility when ceria is doped with copper and the lower cost of copper compared with platinum or palladium (Pt = $1,810/oz, Pd = $789/oz, Cu = $4.35/oz),[44] our results indicate that Cu(II) is a promising ceria dopant as a replacement for Pd(II) or Pt(II). Ceria doped with Zn(II) also shows significant enhanced reducibility, and it is the cheapest of these metals (Zn = $1.10/oz).[44] In fact, it has very recently been shown experimentally that the incorporation of Zn promotes the reduction of CeO_2.[45]

In summary, we have provided a blueprint for the choice of dopants to improve the reducibility of an oxide catalyst. We have highlighted the importance of considering the minimum energy configuration of a doped system and the relaxation experienced by the dopant in the host oxide, which can lead to improved reducibility and enhance the OSC of CeO_2. In general, when selecting dopants to improve the OSC of any material, it is important to consider (a) the dopant ionic radius, which should be small enough to adopt alternative positions in the lattice, (b) the dopant coordination in the respective binary oxide, which should be lower than that of the host ion to create under coordinated or weakly bound oxygen ions, and (c) for transition metals, the driving force of altered crystal-field splitting, which can lead to alternative coordination. The insights gleamed from this study can be used to aid in the design of next generation catalysts.

AUTHOR INFORMATION

Corresponding Author

*E-mail: scanloda@tcd.ie; watsong@tcd.ie.

ACKNOWLEDGMENT

This work was supported by Science Foundation Ireland through the Research Frontiers Programme (grant numbers 08/RFP/MTR1044 and 09/RFP/MTR2274). Calculations were performed on the IITAC, Lonsdale and Kelvin supercomputers as maintained by TCHPC, and the Stokes supercomputer as maintained by ICHEC.

REFERENCES

(1) Trovarelli, A. In *Catalysis by Ceria and Related Materials*; Hutchings, G. J., Ed.; Imperial College Press: London, 2002.

(2) Scanlon, D. O.; Galea, N. M.; Morgan, B. J.; Watson, G. W. *J. Phys. Chem. C* **2009**, *113*, 11095–11103.

(3) Fabris, S.; de Gironcoli, S.; Baroni, S.; Vicario, G.; Gabriele, B. *Phys. Rev. B* **2005**, *71*, 041102.

(4) Trovarelli, A. *Comments Inorg. Chem.* **1999**, *20*, 263.

(5) Skorodumova, N. V.; Simak, S. I.; Lundqvist, B. I.; Abrikosov, I. A.; Johansson, B. *Phys. Rev. Lett.* **2002**, *89*, 166601.

(6) Hegde, M. S.; Madras, G.; Patil, K. C. *Acc. Chem. Res.* **2009**, *42*, 704–712.

(7) Priolkar, K. R.; Bera, P.; Sarode, P. R.; Hegde, M.; Emura, S.; Kamashiro, R.; Lalla, N. P. *Chem. Mater.* **2002**, *14*, 2120–2128.

(8) Gayen, A.; Baidya, T.; Prakash, A. S.; Ravishankar, N.; Hegde, M. S. *Indian J. Chem. A* **2005**, *44A*, 34–48.

(9) Bera, P.; Priolkar, K. R.; Sarode, P. R.; Hegde, M. S.; Emura, S.; Kumashiro, R.; Lalla, N. P. *Chem. Mater.* **2002**, *14*, 3591–3601.

(10) Bera, P.; Aruna, S. T.; Patil, K. C.; Hegde, M. S. *J. Catal.* **1999**, *186*, 36–44.

(11) Harrison, P. G.; Ball, I. K.; Azelee, W.; Daniell, W.; Goldfarb, D. *Chem. Mater.* **2000**, *12*, 3715–3725.

(12) Yisup, N.; Cao, Y.; Feng, W. L.; Dai, W. L.; Fan, K. N. *Catal. Lett.* **2005**, *99*, 207–213.

(13) Jacobs, G.; Chenu, E.; Patterson, P. M.; Williams, L.; Sparks, D.; Thomas, G.; Davis, B. H. *Appl. Catal., A* **2004**, *258*, 203–214.

(14) Wang, X. Q.; Rodriguez, J. A.; Hanson, J. C.; Gamarra, D.; Martinez-Arias, A.; Fernandez-Garcia, M. *J. Phys. Chem. B* **2005**, *109*, 19595–19603.

(15) Chafi, Z.; Keghouche, N.; Minot, C. *Surf. Sci.* **2007**, *601*, 2323–2329.

(16) Yang, Z.; Luo, G.; Lu, Z.; Hermansson, K. *J. Chem. Phys.* **2007**, *127*, 074704.

(17) Yang, Z.; LuO, G.; Lu, Z.; Woo, T. K.; Hermansson, K. *J. Phys: Condens Matt.* **2008**, *20*, 035210.

(18) Wang, X. Q.; Shen, M. Q.; Wang, J.; Fabris, S. *J. Phys. Chem. C* **2010**, *114*, 10221–10228.

(19) Dutta, G.; Waghmare, U. V.; Baidya, T.; Hegde, M. S.; Priolkar, K. R.; Sarode, P. R. *Catal. Lett.* **2006**, *108*, 165–172.

(20) Dutta, G.; Waghmare, U. V.; Baidya, T.; Hegde, M. S.; Priolkar, K. R.; Sarode, P. R. *Chem. Mater.* **2006**, *18*, 3249–3256.

(21) Gupta, A.; Waghmare, U. V.; Hegde, M. S. *Chem. Mater.* **2010**, *22*, 5184–5198.

(22) Scanlon, D. O.; Morgan, B. J.; Watson, G. W. *Phys. Chem. Chem. Phys.* **2011**, *13*, 4279–4284.

(23) Nolan, M. *J. Mater. Chem.* **2011**, *21*, 9160–9168.

(24) Kresse, G.; Hafner, J. *Phys. Rev. B* **1994**, *49*, 14251–14271.

(25) Perdew, J. P.; Burke, K.; Ernzerhof, M. *Phys. Rev. Lett.* **1996**, *77*, 3865–3868.

(26) Dudarev, S. L.; Botton, G. A.; Savrasov, S. Y.; Humphreys, C. J.; Sutton, A. P. *Phys. Rev. B* **1998**, *57*, 1505–1509.

(27) Nolan, M.; Grigoleit, S.; Sayle, D. C.; Parker, S. C.; Watson, G. W. *Surf. Sci.* **2005**, *576*, 217–229.

(28) Nolan, M.; Parker, S. C.; Watson, G. W. *Surf. Sci.* **2005**, *595*, 223–232.

(29) Morgan, B. J.; Watson, G. W. *Surf. Sci.* **2007**, *601*, 5034–5041.

(30) Scanlon, D. O.; Walsh, A.; Morgan, B. J.; Watson, G. W. *J. Phys. Chem. C* **2008**, *112*, 9903–9911.

(31) Morgan, B. J.; Scanlon, D. O.; Watson, G. W. *J. Mater. Chem.* **2009**, *19*, 5175–5178.

(32) Keating, P. R. L.; Scanlon, D. O.; Watson, G. W. *J. Phys.: Condens. Matter* **2009**, *21*, 405502.

(33) Galea, N. M.; Scanlon, D. O.; Morgan, B. J.; Watson, G. W. *Mol. Sim.* **2009**, *35*, 577–583.

(34) Nolan, M.; Parker, S. C.; Watson, G. W. *Surf. Sci.* **2006**, *600*, L175–L178.

(35) Keating, P. R. L.; Morgan, B. J.; Scanlon, D. O.; Watson, G. W. *J. Phys. Chem. C* **2011**In Submission.

(36) Scanlon, D. O.; Walsh, A.; Morgan, B. J.; Watson, G. W.; Payne, D. J.; Egdell, R. G. *Phys. Rev. B* **2009**, *79*, 035101.

(37) Scanlon, D. O.; Morgan, B. J.; Watson, G. W. *J. Chem. Phys.* **2009**, *131*, 124703.

(38) Arnold, T.; Payne, D. J.; Bourlange, A.; Hu, J. P.; Egdell, R. G.; Piper, L. F. J.; Colakerol, L.; De Masi, A.; Glans, P. A.; Learmonth, T.; Smith, K. E.; Guo, J.; Scanlon, D. O.; Walsh, A.; Morgan, B. J.; et al. *Phys. Rev. B* **2009**, *79*, 075102.

(39) Ferrari, A. M.; Pisani, C.; Cinquini, F.; Giordano, L.; Pacchioni, G. *J. Chem. Phys.* **2007**, *127*, 174711.

(40) Pillo, T.; Zimmermann, R.; Steiner, P.; Hufner, S. *J. Phys.: Condensed Matter* **1997**, *9*, 3987–3999.

(41) Scanlon, D. O.; Walsh, A.; Morgan, B. J.; Nolan, M.; Fearon, J.; Watson, G. W. *J. Phys. Chem. C* **2007**, *111*, 7971–7979.

(42) Schirmer, O. F. *J. Phys.: Condens. Matter* **2006**, *18*, R667–R704.

(43) Lu, Z.; Yang, Z.; He, B.; Castleton, C.; Hermansson, K. *Chem. Phys. Lett.* **2011**, *519*, 60−66.

(44) http://www.metalprices.com/

(45) Ying, L.; Liu, J.; Mo, L.; Lou, H.; Zheng, X. *Int.J. Hydrogen Energy* **2011**, DOI: 10.1016/j.ijhydene.2011.03.054.